

Quantum phase transition in ferroelectric-paraelectric heterostructures

Prasanna Venkatesan Ravindran^{1, a)} and Asif Islam Khan^{1, 2}

¹⁾*School of Electrical and Computer Engineering, Georgia Institute of Technology, Atlanta, GA 30332, USA*

²⁾*School of Materials Science and Engineering, Georgia Institute of Technology, Atlanta, GA 30332, USA*

Phase transition between ferroelectricity and quantum paraelectricity via non-thermal tuning parameters can lead to quantum critical behavior and associated emergent phenomena. Ferroelectric quantum critical systems are, however, rare despite the abundance of ferroelectric materials. Here, we show theoretically that in ferroelectric-paraelectric heterostructures, it is plausible to induce quantum paraelectricity where the quantum temperature (*i.e.*, the temperature below with the onset of ferroelectricity is suppressed by quantum fluctuations) can be tuned by the thickness ratio. This, in turn, can effect a quantum phase transition between effective ferroelectric and quantum paraelectric states, using the thickness ratio as the tuning parameter. The associated quantum critical region offers unexpected prospects in the field of ferroelectric quantum criticality.

^{a)}pvr@gatech.edu

Ferroelectric materials are, in general, known to obey the Curie-Weiss law, relating the dielectric constant ϵ and the temperature T , given as

$$\epsilon = \frac{M}{T - T_C} \quad (1)$$

where M is the Curie constant, and T_C is the temperature for the paraelectric-ferroelectric phase transition, *i.e.*, the Curie temperature. Barrett, in 1952¹, suggested a modification to this law by extending Slater's statistical treatment of ferroelectricity² to include quantum mechanical effects. This leads to a quantum statistical relation between ϵ and T , known as the Barrett's formula, which is given as

$$\epsilon = \frac{M}{\frac{1}{2}T_1 \coth\left(\frac{T_1}{2T}\right) - T_C} \quad (2)$$

where T_1 is a quantum temperature, given by $T_1 = \hbar\omega/k_B$, with \hbar , k_B and $\hbar\omega$ being the reduced Planck constant, the Boltzmann constant and twice the zero point energy of the harmonic part of the potential energy of the dipole, respectively. When T_C is much larger than T_1 , Barrett's formula reduces to the Curie-Weiss law (Eq. 1). On the other hand, if $T_C < T_1$, the material exhibits non-Curie-Weiss behavior. More importantly, if $T_C < T_1/2$, the function: $\epsilon(T)$ lacks a singularity, indicating that there is no paraelectric-ferroelectric phase transition in the system and that the material behaves as a paraelectric in the entire temperature range. The suppression of ferroelectricity below T_C occurs due to the dominance of quantum fluctuations (zero-point motion) over their thermal counterparts, and hence the phenomenon is often referred to as quantum paraelectricity.

Recent interests in quantum paraelectricity lie in the context of quantum phase transition and quantum criticality.³⁻⁵ In the limit of zero temperature where thermal fluctuations are absent, phase transition with respect to a non-thermal tuning parameter, g , such as pressure, composition and so on, can be driven purely by quantum fluctuations. Quantum phase transitions, as they are referred to⁶, are most commonly observed in magnets⁷⁻⁹, superconductors and cold atomic/2-D bosonic gases.^{10,11} The associated quantum critical point, separating the quantum phases, lies on the 0 K line in the T vs. g phase diagram — however, the influence of quantum phase transition extends above 0 K into the finite temperatures forming the quantum critical region (Fig. 1). In this region, the interplay between quantum and thermal fluctuations can lead to novel, unexpected and exotic phenomena, and phases of matter. The most well-known examples of quantum critical behavior are the emergence of unconventional superconductivity⁸ and 'strange' metallicity.^{12,13}

Composition¹⁴, isotopic substitution¹⁵ and pressure¹⁶ have been explored as the tuning parameters to access the ferroelectric quantum critical region in SrTiO₃ (STO), the earliest and the most well-known quantum paraelectric. In fact, ferroelectric quantum criticality has theoretically been shown as the origin of superconductivity in doped variants of STO.¹⁷ Furthermore, spin can be added to quantum paraelectrics as an additional degree of freedom leading to multiferroics that exhibit a rich quantum critical behavior around the quantum critical point.⁴ All told, ferroelectric quantum critical systems are rare. This is despite that ferroelectrics are one of the largest classes of functional materials that includes perovskite oxides,¹⁸ organic polymers¹⁹, fluorite-structure oxides²⁰ and layered and two-dimensional materials²¹, and so on, and that quite a few quantum paraelectric materials are known to exist (see supplementary table S1 for the relative values of $T_1/2$ and T_C for different materials). The rarity of ferroelectric quantum critical system is due to the fact that for quantum criticality, a facile tuning parameter is required that can tune the relative values of $T_1/2$ and T_C — which may not be generally available for a wide range of materials.

To that effect, ferroelectric–paraelectric heterostructures, especially in superlattice forms, have been a rich and diverse playground to tune phase transitions — by mediating the interplay between strain, electrostatics and interfacial effects through careful heterostructure design and epitaxial growth with single atomic layer precision.^{22–30} Dramatic control of functional properties, such as polarization, capacitance, Curie temperature and so on by superlattice period and thickness ratio has been demonstrated in these structures. Recent observation of intricate superstructures containing nanometric polarization textures, namely polar vortices²⁶ and skyrmions²⁸, and functional features therein, such as high-frequency collective responses³¹, chiral and toroidal order^{32,33}, local static negative dielectric permittivity^{27,29}, and so on has spring-boarded renewed interests in these systems.

In this letter, we discuss the possibility of utilizing heterostructuring to access the quantum critical region, in otherwise ferroelectric materials by tuning the effective Curie temperature. Using a combination of analytical and numerical approaches, we show that it is plausible to engineer quantum paraelectricity in ferroelectric-paraelectric heterostructures. In doing so, quantum critical behavior can emerge in such heterostructures, where the thickness ratio between the paraelectric and the ferroelectric layers is the tuning parameter.

To begin with, the Gibbs free energy per unit volume of a ferroelectric material, U_F , can be phenomenologically expressed as an even order polynomial of the order parameter P ,

given as

$$U_F = \frac{1}{2\epsilon(T)}P^2 + \sum_{i=2,\dots} \alpha_i P^{2i} \quad (3)$$

where α_i are anisotropy constants, temperature independent, and considered positive in this work. In the standard Landau phenomenology of ferroelectricity, ϵ is given by Eq. 1. To consider quantum effects, it will be given by Eq. 2 in this work. If $T_C > T_1/2$, the energy profile — the U_F vs. P curve — of the ferroelectric has a double-well shape at $T < T_C$, as shown in Fig. 2(a). We make an assumption, for the sake of simplicity, with regards to a ferroelectric-paraelectric heterostructure that the polarization is restricted to a direction perpendicular to the interfaces and is spatially homogeneous. A paraelectric is characterized by a single well energy profile $U_P = P^2/2\epsilon_P$, U_P and ϵ_P being the free energy per unit volume and dielectric permittivity of the paraelectric material, respectively. The free energy per unit area of the FE-PE structure is a linear combination of the free energy densities of individual layers: $t_F U_F(P) + t_P U_P(P)$, where t_F and t_P are the thicknesses of the ferroelectric layer and the paraelectric layer, respectively. At a given temperature, the functional response of the FE-PE heterostructure can be tuned by the relative values of t_F and t_P , as shown in Fig. 2. If the curvature of $t_P U_P(P)$ profile is smaller than the magnitude of the negative curvature of the $t_F U_F(P)$ profile at $P = 0$, the energy profile, $U(P)$, retains a double-well shape, resulting in a functional ferroelectric response (Fig. 2(b)). On the other hand, if the curvature of $t_P U_P(P)$ profile is larger than the magnitude of the negative curvature of the $t_F U_F(P)$ profile at $P = 0$, the energy profile, $U(P)$, has a single-well shape, leading to a functional paraelectric response (Fig. 2(c)). The free energy density per unit volume of the ferroelectric-paraelectric heterostructure, U , is given as

$$U = \frac{t_F U_F + t_P U_P}{t_F + t_P} = \frac{1}{2\epsilon'(T)}P^2 + \sum_{i=2,\dots} \alpha_i P^{2i} \quad (4)$$

where ϵ' is the effective dielectric constant of the FE-PE layer. ϵ' has the same functional form as that in Eq. 2, except that T_C is replaced by an effective Curie temperature T'_C , given as

$$T'_C = T_C - \frac{M}{\epsilon_P} r \quad (5)$$

where, r is the ratio between the thicknesses of the paraelectric and the ferroelectric layers ($r = t_P/t_F$). According to Eq. 5, the effect of adding a paraelectric material to or increasing its fraction in a ferroelectric heterostructure is to cause an apparent reduction of the Curie temperature. The temperature at which the paraelectric-ferroelectric transition, $T_{P\leftrightarrow F}$, occurs can be calculated by finding the pole of $1/\epsilon'(T)$, which is given as

$$T_{P\leftrightarrow F} = \frac{T_1}{2 \coth^{-1} \frac{2T'_C(r)}{T_1}} \quad (6)$$

Note in Eq. 6 that if $T'_C \gg T_1/2$, $T_{P\leftrightarrow F}$ and T'_C coincides. On the other hand, by setting $T_{P\leftrightarrow F}=0$, one gets the condition for which ferroelectricity is suppressed at 0 K in the ferroelectric-paraelectric heterostructure, making its functional response equivalent to that of a quantum paraelectric. The critical thickness ratio, r_C , above which the FE-PE heterostructure transition from being a ferroelectric to a quantum paraelectric (*i.e.*, $T'_C < T_1/2$) is found to be

$$r_C = \frac{\epsilon_P}{M} \left(T_C - \frac{T_1}{2} \right) \quad (7)$$

$r = r_C$ represents a quantum critical point between the ferroelectric and the quantum paraelectric phase in the ferroelectric-paraelectric structure.

To obtain quantitative values of the phenomenological parameters in Eq. 3, we fit the expression to the numerical solution of quantum statistical model of the ferroelectric, which is specified by T_1 , T_C and M . In this quantum model, similar to the procedure presented in Barrett,¹ it is assumed that in a single unit cell of the displacement-type ferroelectric, only the ion at the body center moves and that it moves only along the vertical axis, allowing the unit cell to be treated as an anharmonic oscillator. The potential energy of the displaced body-center ion under electric field E , is given by $\phi(x) = ax^2 + bx^4 - qx E$. The partition function z of a single oscillator is: $z = \sum_{n=1}^{\infty} \exp(-\epsilon_n/k_B T)$, where ϵ_n is the n -th quantized energy level of the oscillator. The partition function for a system of N oscillators, $Z = z^N/N!$. The equivalent Helmholtz free energy in terms of the electric field is given by $A_E = -k_B T \log Z$. The ionic polarizability of the body-center ion is $\alpha' = (\partial P/\partial E)/N$, with P being the order parameter: polarization, given as $P = -(\partial A_E/\partial E)_T$. The free energy of the ferroelectric material with independent body-center ions, A_P calculated as $A_P = A_E + PE$, can be expressed as $A_P = \alpha' P^2 + \beta' P^4$. The interaction of ions with each

other is taken into account using Lorentz correction.² For Lorentz correction constants, c_3 and c_4 , the Gibbs free energy per unit volume of the ferroelectric, $A_P = \alpha P^2 + \beta P^4$, with α and β being given by

$$\alpha = c_3^2 \alpha' + \frac{c_3 c_4}{2\epsilon_0} \quad (8)$$

$$\beta = c_3^3 \beta' \quad (9)$$

For a perovskite crystal structure, c_3 and c_4 were calculated by Slater.² The procedure to calculate the microscopic parameters a and b , and the Lorentz correction terms c_3 and c_4 for given values of T_1 , T_C and M is detailed in the supplementary section I.

For numerical calculations, the material parameters for the heterostructures are as follows: $T_1/2=25$ K, $T_C=390$ K, $M=1.5 \times 10^5$ K $\times \epsilon_o$, and $\epsilon_P=200\epsilon_o$, where ϵ_o is the vacuum permittivity. The microscopic parameters (a , b , c_3 and c_4) calculated for these values are listed in supplementary table S1. Fig. 3(a) and 3(b) plot $1/\epsilon'$ and the remanent polarization P_o as functions of T of the ferroelectric-paraelectric heterostructure for different values of r . The shift of T'_C with an increasing r is observed. For $r = 0.5$, 0.52 and 0.7, $1/\epsilon'$ vs. T curves flatten out for $T < T_1/2$, and P_o is zero at all temperatures. Fig. 3(c) and 3(d) show phase plots of P_o and $1/\epsilon'$ in the (T, r) plane, respectively. In Fig. 3(c), the boundary between $P_o \neq 0$ and $P_o = 0$ regions represents the $T_{P \leftrightarrow F}$ contour. At the zero-temperature limit ($T=0$ K), the ferroelectric to paraelectric transition occurs at $r = 0.49$, which represents the quantum critical point, r_C .

Fig. 4 plots $T_{P \leftrightarrow F}$ and T'_C as functions of r . We observe that $T_{P \leftrightarrow F}$ follows T'_C until $T'_C \approx T_1$, and $T_{P \leftrightarrow F} = 0$ K, when $T'_C = T_1/2$. Note that $T'_C = 0$ K at $r = 0.52$, and for $r > 0.52$, the ferroelectric-paraelectric heterostructure would have exhibited paraelectricity at all temperatures — even in the classical case (*i.e.*, in the hypothetical case where quantum fluctuations are absent). While quantum effects manifest for all value of r in the form of slowly varying ϵ' and P_o at $T < T_1/2$ (as seen in Fig. 3(a) and 3(b), respectively), it is only in the range $r \in (r_C, \epsilon_P T_C / M)$ that quantum fluctuations suppress ferroelectricity that would have been present in the classical scenario.

So far, we considered the paraelectric to have a temperature-independent dielectric permittivity, for the sake of providing an intuitive picture of the quantum phase transition in the system. We also modeled the heterostructures where the paraelectric has a temperature

dependence, *e.g.* governed by the Barrett formula. Supplementary Fig. S3(a) and S3(b) show the phase plots of P_0 and $1/\epsilon'$, respectively, in the $(T - r)$ plane for a $\text{BaTiO}_3(\text{BTO})$ - $\text{SrTiO}_3(\text{STO})$ heterostructure. We also varied the parameters of the ferroelectric and the paraelectric to understand their impact on the phase diagram, a few examples of which are shown in Fig. S3(c-f). In all cases, we observe that the phase diagrams show clear boundaries between the ferroelectric, the paraelectric and the quantum paraelectric phases and the quantum critical points.

By varying the quantum temperature of the paraelectric, $T_{1,P}$, while keeping that of the ferroelectric, $T_{1,F}$, a constant for different value of r , we observe that the effective T_1 in a ferroelectric-paraelectric heterostructure, $T_{1,FP}$, lies between $T_{1,F}$ and $T_{1,P}$ (Fig. 5). This indicates that in addition to the effective Curie temperature (T'_C), the quantum temperature of the ferroelectric-paraelectric heterostructure is also tunable by the thickness ratio.

It is encouraging to note that, experimentally, tens to hundreds of K of shift in the effective Curie temperature with the change of the individual layer thicknesses has been observed in $\text{PbTiO}_3/\text{SrTiO}_3$, $\text{BaTiO}_3/\text{SrTiO}_3$ and $\text{PbSrTiO}_3/\text{SrTiO}_3$ superlattices.^{23–25,34–36} This indicates that classical phase transition occurs in these systems where thickness ratio is the tuning parameter. Electric displacement in such structures is spatially non-uniform, leading to intricate polarization textures, such as 180° domains³⁴, polar vortices²⁶ and skyrmions²⁸ — all of which are also strongly affected by the epitaxial strain. Admittedly, studies into these exciting phenomena are, however, limited to the classical regime, away from the quantum limits in the cryogenic temperature range. These effects, which are not considered in our theoretical analysis, can add richness to the predicted quantum critical region in ferroelectric-paraelectric heterostructures.

In summary, we have discussed the possibility of a quantum paraelectric phase in ferroelectric heterostructures. Further we have also presented the possibility of achieving tunable quantum paraelectricity in ferroelectric-paraelectric heterostructure, where the quantum temperature, the temperature below which the onset of an effective ferroelectricity is suppressed due to quantum fluctuations, and the transition temperature from ferroelectric to quantum paraelectric phase — can be tuned by the thickness ratio. This raises the prospect of observing quantum phase transition and a quantum critical region in such systems, with the thickness ratio as the tuning parameter. Experiments geared at elucidating if a quantum phase transition is indeed present in the zero-temperature limit in these heterostructures and

at extracting the scaling laws that characterize the ferroelectric quantum critical regime are an exciting avenue for future research.

This work was supported by the Georgia Tech Quantum Alliance (GTQA). The authors thank Jayakanth Ravichandran and Martin Mourigal for fruitful discussions.

REFERENCES

- ¹J. H. Barrett, Physical Review **86**, 118 (1952).
- ²J. Slater, Physical Review **78**, 748 (1950).
- ³S. Rowley, L. Spalek, R. Smith, M. Dean, M. Itoh, J. Scott, G. Lonzarich, and S. Saxena, Nature Physics **10**, 367 (2014).
- ⁴A. Narayan, A. Cano, A. V. Balatsky, and N. A. Spaldin, Nature materials **18**, 223 (2019).
- ⁵P. Chandra, G. G. Lonzarich, S. Rowley, and J. Scott, Reports on Progress in Physics **80**, 112502 (2017).
- ⁶S. Sachdev, Handbook of Magnetism and Advanced Magnetic Materials (2007).
- ⁷H. v. Löhneysen, A. Rosch, M. Vojta, and P. Wölfle, Reviews of Modern Physics **79**, 1015 (2007).
- ⁸P. Gegenwart, Q. Si, and F. Steglich, nature physics **4**, 186 (2008).
- ⁹P. A. Volkov and P. Chandra, Physical review letters **124**, 237601 (2020).
- ¹⁰M. Endres, T. Fukuhara, D. Pekker, M. Cheneau, P. Schauβ, C. Gross, E. Demler, S. Kuhr, and I. Bloch, Nature **487**, 454 (2012).
- ¹¹A. Rançon and N. Dupuis, EPL (Europhysics Letters) **104**, 16002 (2013).
- ¹²I. M. Hayes, N. Maksimovic, G. N. Lopez, M. K. Chan, B. Ramshaw, R. D. McDonald, and J. G. Analytis, Nature Physics **17**, 58 (2021).
- ¹³S. Sachdev and B. Keimer, arXiv preprint arXiv:1102.4628 (2011).
- ¹⁴C. W. Rischau, X. Lin, C. P. Grams, D. Finck, S. Harms, J. Engelmayer, T. Lorenz, Y. Gallais, B. Fauque, J. Hemberger, *et al.*, Nature Physics **13**, 643 (2017).
- ¹⁵M. Itoh and R. Wang, Applied Physics Letters **76**, 221 (2000).
- ¹⁶M. J. Coak, C. R. S. Haines, C. Liu, G. G. Guzmán-Verri, and S. S. Saxena, Physical Review B **100**, 214111 (2019).
- ¹⁷J. M. Edge, Y. Kedem, U. Aschauer, N. A. Spaldin, and A. V. Balatsky, Physical review letters **115**, 247002 (2015).
- ¹⁸M. E. Lines and A. M. Glass, *Principles and applications of ferroelectrics and related materials* (Oxford university press, 2001).
- ¹⁹A. V. Bune, V. M. Fridkin, S. Ducharme, L. M. Blinov, S. P. Palto, A. V. Sorokin, S. Yudin, and A. Zlatkin, Nature **391**, 874 (1998).
- ²⁰T. Böske, S. Teichert, D. Bräuhaus, J. Müller, U. Schröder, U. Böttger, and T. Mikolajick,

- Applied Physics Letters **99**, 112904 (2011).
- ²¹F. Liu, L. You, K. L. Seyler, X. Li, P. Yu, J. Lin, X. Wang, J. Zhou, H. Wang, H. He, *et al.*, Nature communications **7**, 1 (2016).
- ²²H. N. Lee, H. M. Christen, M. F. Chisholm, C. M. Rouleau, and D. H. Lowndes, Nature **433**, 395 (2005).
- ²³E. Bousquet, M. Dawber, N. Stucki, C. Lichtensteiger, P. Hermet, S. Gariglio, J.-M. Triscone, and P. Ghosez, Nature **452**, 732 (2008).
- ²⁴D. Tenne, A. Bruchhausen, N. Lanzillotti-Kimura, A. Fainstein, R. Katiyar, A. Cantarero, A. Soukiassian, V. Vaithyanathan, J. Haeni, W. Tian, *et al.*, Science **313**, 1614 (2006).
- ²⁵M. Dawber, N. Stucki, C. Lichtensteiger, S. Gariglio, P. Ghosez, and J.-M. Triscone, Advanced Materials **19**, 4153 (2007).
- ²⁶A. Yadav, C. Nelson, S. Hsu, Z. Hong, J. Clarkson, C. Schlepütz, A. Damodaran, P. Shafer, E. Arenholz, L. Dedon, *et al.*, Nature **530**, 198 (2016).
- ²⁷A. K. Yadav, K. X. Nguyen, Z. Hong, P. García-Fernández, P. Aguado-Puente, C. T. Nelson, S. Das, B. Prasad, D. Kwon, S. Cheema, *et al.*, Nature **565**, 468 (2019).
- ²⁸S. Das, Y. Tang, Z. Hong, M. Gonçalves, M. McCarter, C. Klewe, K. Nguyen, F. Gómez-Ortiz, P. Shafer, E. Arenholz, *et al.*, Nature **568**, 368 (2019).
- ²⁹S. Das, Z. Hong, V. Stoica, M. Gonçalves, Y.-T. Shao, E. Parsonnet, E. J. Marks, S. Saremi, M. McCarter, A. Reynoso, *et al.*, Nature materials **20**, 194 (2021).
- ³⁰Q. Li, V. A. Stoica, M. Paściak, Y. Zhu, Y. Yuan, T. Yang, M. R. McCarter, S. Das, A. K. Yadav, S. Park, *et al.*, Nature **592**, 376 (2021).
- ³¹K.-S. Li, P.-G. Chen, T.-Y. Lai, C.-H. Lin, C.-C. Cheng, C.-C. Chen, Y.-J. Wei, Y.-F. Hou, M.-H. Liao, M.-H. Lee, *et al.*, in *2015 IEEE International Electron Devices Meeting (IEDM)* (IEEE, 2015) pp. 22–6.
- ³²P. Behera, M. A. May, F. Gómez-Ortiz, S. Susarla, S. Das, C. T. Nelson, L. Caretta, S.-L. Hsu, M. R. McCarter, B. H. Savitzky, *et al.*, arXiv preprint arXiv:2105.14109 (2021).
- ³³A. R. Damodaran, J. Clarkson, Z. Hong, H. Liu, A. K. Yadav, C. T. Nelson, S.-L. Hsu, M. McCarter, K.-D. Park, V. Kravtsov, *et al.*, Nature materials **16**, 1003 (2017).
- ³⁴P. Zubko, N. Stucki, C. Lichtensteiger, and J.-M. Triscone, Physical Review Letters **104**, 187601 (2010).
- ³⁵P. Zubko, N. Jecklin, N. Stucki, C. Lichtensteiger, G. Rispens, and J.-M. Triscone, Ferroelectrics **433**, 127 (2012).

³⁶P. Zubko, J. C. Wojdeł, M. Hadjimichael, S. Fernandez-Pena, A. Sené, I. Luk'yanchuk, J.-M. Triscone, and J. Íñiguez, *Nature* **534**, 524 (2016).

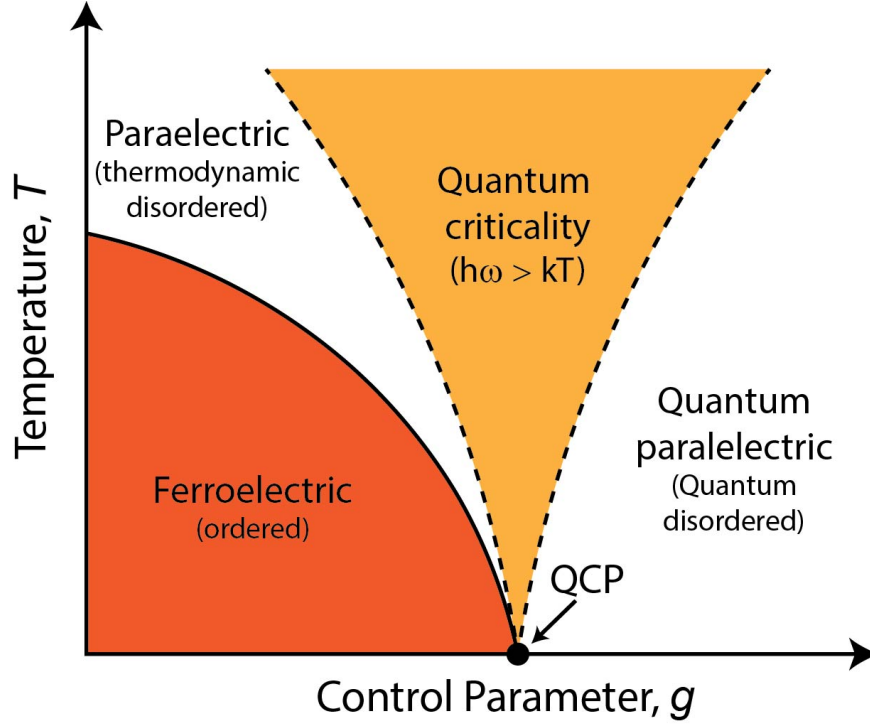


FIG. 1. **Temperature-Control Parameter Phase diagram:** Phase diagram at the ferroelectric-quantum paraelectric phase transition. At 0 K, where thermally no phase transition is possible. But tuning a physical parameter could facilitate quantum fluctuations to suppress the ferroelectric order causing a phase transition from ferroelectric to a quantum paraelectric phase, giving rise to a quantum critical point. Counter intuitively, the effect of quantum fluctuations extends to larger ranges of the control parameter as temperature increases, leading to a quantum critical region where $\hbar\omega > kT$. This region is filled with exciting effects ranging from superconductivity to polar metallicity.^{8,9}

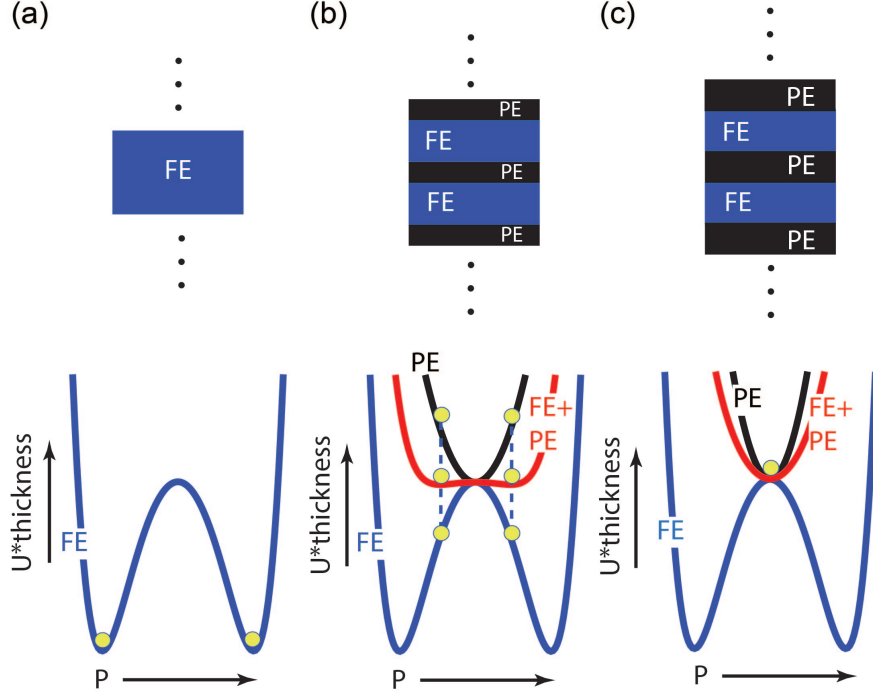


FIG. 2. (a) **Free energy of a stand-alone ferroelectric layer:** The double well energy landscape of a ferroelectric with $T_C > T_1/2$ at $T > T_C$. (b) **Free energy of a FE-PE heterostructure with an effective ferroelectric phase:** the positive curvature at $P = 0$ due to the paraelectric is less than the magnitude of the negative curvature due to the ferroelectric phase. (c) **Free energy of a FE-PE heterostructure with an effective paraelectric phase:** the positive curvature at $P = 0$ due to the paraelectric is more than the magnitude of the negative curvature due to the ferroelectric phase

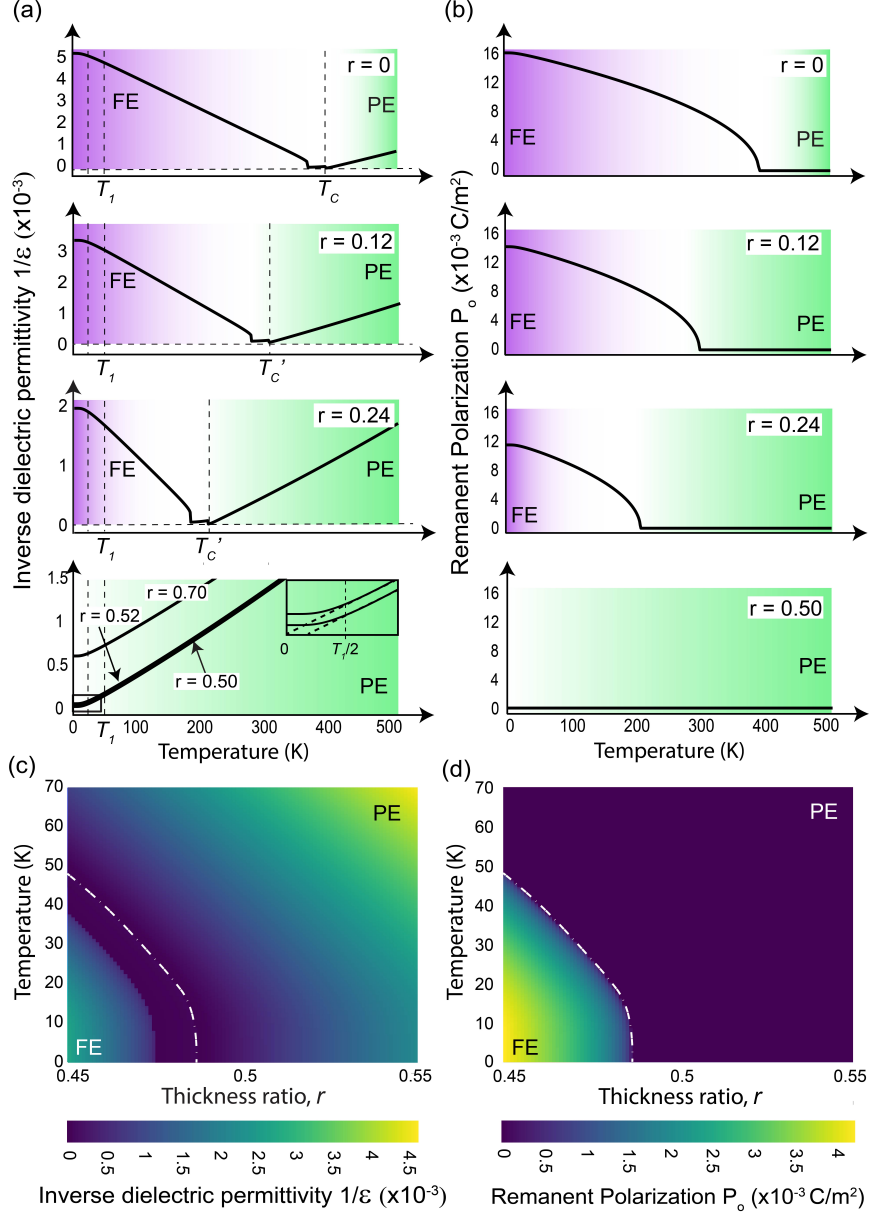


FIG. 3. **(a) Inverse dielectric permittivity and (b) Remanent Polarization:** Variation of the inverse dielectric permittivity and remanent polarization with temperature is shown for different values of thickness ratio illustrating the decrease in transition temperature with increasing r . When $r > r_C$, T'_C reduces below $T_1/2$ and the heterostructure becomes a quantum paraelectric as shown in the inset in (a) and the zero-remnant polarization. For $r > \epsilon_P T_C / M$, the heterostructure becomes a paraelectric with $T'_C < 0$. **(c&d) Ferroelectric-Paraelectric Phase Diagrams:** Temperature-thickness ratio phase diagrams show the (c) inverse dielectric permittivity and (b) remanent polarization of the heterostructure. The white line represents the phase boundary between the ferroelectric and paraelectric phases.

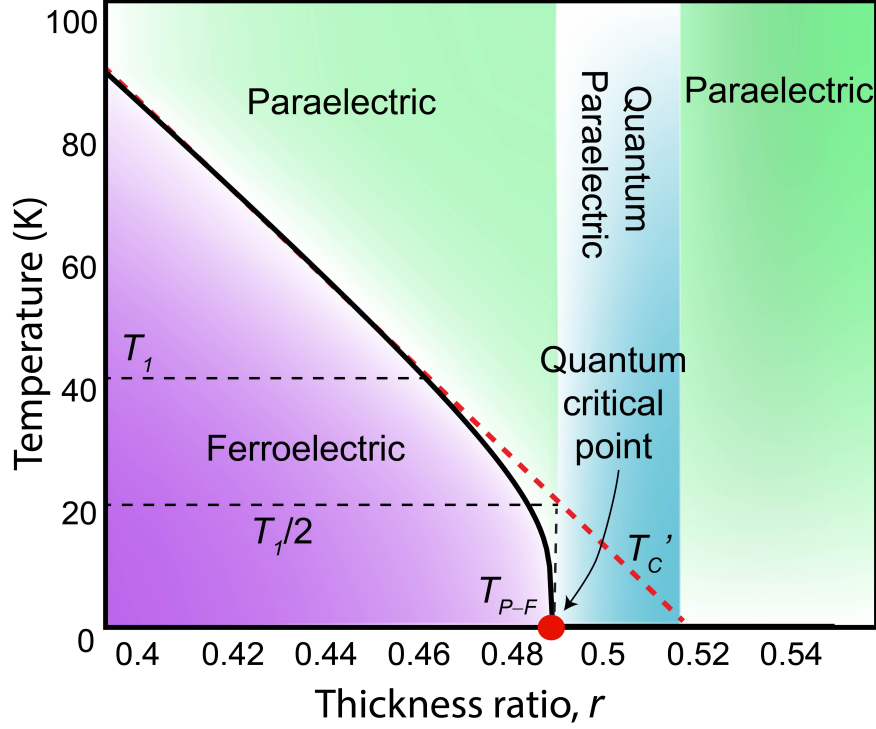


FIG. 4. **Temperature-Thickness ratio phase diagram:** The T-r plane shows the phase transition from ferroelectric to quantum paraelectric phase. The phase transition is tuned by the ratio of thickness of the paraelectric and ferroelectric layers, r . At 0 K, the heterostructure transitions from a ferroelectric to quantum paraelectric phase at $r = r_C$, the quantum critical point. The system remains in this incipient ferroelectric phase for r ranging from r_C to $\epsilon_P T_C / M$. For $r > \epsilon_P T_C / M$, the heterostructure acts as a paraelectric for any temperature as predicted by the classical theory.

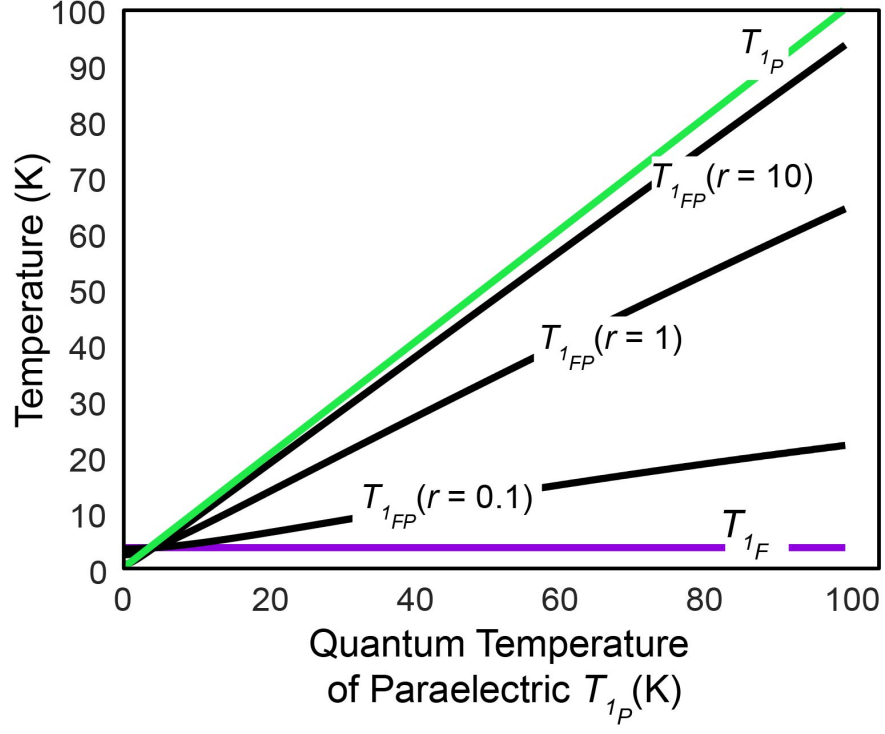


FIG. 5. The effective quantum temperature $T_{1_{FP}}$ of the FE-PE heterostructure with the ferroelectric as BTO and a paraelectric layer with $M_P = 1.55 \times 10^5 \times \epsilon_0$ K and T_{1_P} varying from 0.1 K to 100 K is shown for different thickness ratios.

Quantum phase transition in ferroelectric-paraelectric heterostructures

Prasanna Venkatesan Ravindran^{1,*} and Asif Islam Khan^{1,2}

¹*School of Electrical and Computer Engineering,
Georgia Institute of Technology, Atlanta, GA 30332, USA*

²*School of Materials Science and Engineering,
Georgia Institute of Technology, Atlanta, GA 30332, USA*

arXiv:2203.02058v1 [cond-mat.mes-hall] 3 Mar 2022

* pvr@gatech.edu

I. MICROSCOPIC PARAMETERS AND LORENTZ PARAMETERS

The polarization from a single unit cell is given described by the spring constants, a and b and the Lorentz parameters, c_3 and c_4 . For a ferroelectric whose macroscopic dielectric permittivity is given by Eq. 2 can be described by the macroscopic parameters, M , T_1 and T_C . All these parameters are related by the following equations:[1, 2]

$$T_1 = \frac{\hbar\nu}{k} \quad (\text{S1})$$

$$\nu = \sqrt{\frac{2a}{m}} \quad (\text{S2})$$

$$T_0 = \frac{2a^3\epsilon}{3Nq^2bkD} \left(\frac{Dq^2N}{2a\epsilon} - 1 \right) \quad (\text{S3})$$

$$M = \frac{2a^3\epsilon B}{3Nq^2bkD} \quad (\text{S4})$$

$$b \approx a/10^{-20} \quad (\text{S5})$$

$$B = -\frac{1}{c_3c_4} \quad (\text{S6})$$

$$D = -\frac{c_4}{c_3} \quad (\text{S7})$$

The microscopic parameters and the Lorentz factors for a few ferroelectrics are shown in the table 1. The T_1 value for BaTiO₃ and PbTiO₃ was calculated from the Fig. S1 in ref. [3]. Assuming the dielectric permittivity of the paraelectric to be independent of the temperature, T_1 is the effective Curie temperature of the material for which $r - r_C = 0$. Table S2 shows the classification of the materials based on the relative values of $T_1/2$ and T_C .

II. QUANTUM-STATISTICAL MODEL

A displacive ferroelectric is modeled as follows:

1. Hamiltonian of a unit cell modeled as an anharmonic oscillator(Fig. S2) is given by:

$$\phi(x) = ax^2 + bx^4 - qx E \quad (\text{S8})$$

2. The Schrodinger's equation for the anharmonic oscillator is solved to obtain the quan-

tized energy levels:

$$\phi\psi = \epsilon\psi \quad (\text{S9})$$

3. The partition function z for a single unit cell is given by:

$$z = \sum_{n=1}^{\infty} \exp(-\epsilon_n/k_B T) \quad (\text{S10})$$

4. The partition function is extended to N unit cells giving the partition function of the system:

$$Z = z^N/N! \quad (\text{S11})$$

5. From the partition function of the system, the equivalent Helmholtz free energy A_E is calculated:

$$A_E = -k_B T \log Z \quad (\text{S12})$$

6. The order parameter, P is calculated by taking the first derivative of the Helmholtz free energy:

$$P = -(\partial A_E/\partial E)_T \quad (\text{S13})$$

7. The equivalent Gibbs free energy A_P is calculated from A_E and P :

$$A_P = A_E + PE \quad (\text{S14})$$

TABLE S1. Microscopic parameters and Lorentz correction factors of displacive ferroelectrics. FE₁ is the model ferroelectric used for the numerical calculations in the manuscript.

Material	$T_1/2$ (K)	T_C (K)	M/ϵ_0 (K)	m (kg)	a (N/m)	c_3	c_4
KTaO ₃ [4]	25.67	11.8	6x10 ⁴	3.00x10 ⁻²²	6.7648x10 ³	0.3019	-90.1971
SrTiO ₃ [4]	33.1	24.5	1.55x10 ⁵	7.95x10 ⁻²³	2.9806x10 ³	0.1878	-24.7259
EuTiO ₃ [5]	81	-25	2.34x10 ⁴	7.95x10 ⁻²³	1.7849x10 ⁴	0.4835	-381.0874
NaMnF ₃ [6]	80	-7	4.35x10 ³	9.12x10 ⁻²³	1.9974x10 ⁴	1.1214	-989.0665
BaFe ₁₂ O ₁₉ [7]	23.65	-22.9	-	-	-	-	-
BaTiO ₃ [2, 3]	2.2	390	1.5x10 ⁵	7.95x10 ⁻²³	1.3167x10 ¹	0.1675	-0.1110
PbTiO ₃ [3, 8]	2.9	765	1.5x10 ⁵	7.95x10 ⁻²³	2.28795x10 ¹	0.1645	-0.1929
FE ₁	25	390	1.5x10 ⁵	8.00x10 ⁻²³	1.711x10 ³	0.1908	-14.4285

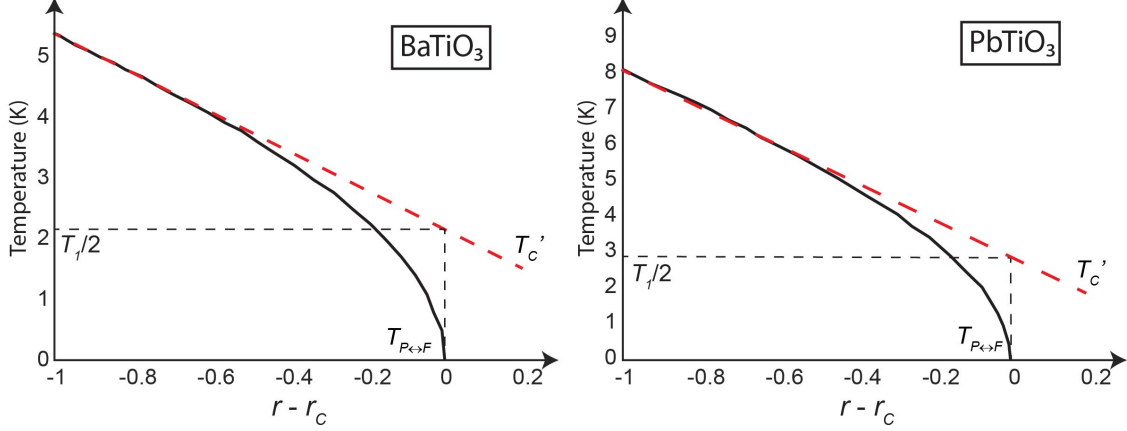


FIG. S1. Variation of the transition temperature $T_{P\leftrightarrow F}$ as a function of pressure for (a) BaTiO_3 and (b) PbTiO_3 is shown by the solid black curve from Fig. 8 in Ref.[3]. The x-axis is the pressure represented as $r - r_C$, where r_C is the pressure at the quantum critical point of the phase transition. The red dashed line shows the variation of effective Curie temperature T'_C with pressure. the dielectric permittivity of the paraelectric to be independent of the temperature, the effective Curie temperature when $r = r_C$ is the half of the quantum temperature $T_1/2$.

8. A_P as a function of P is obtained by fitting $A_P(E)$ to $\alpha'P(E)^2 + \beta'P(E)^4$:

$$A_P(P) = \alpha'P^2 + \beta'P^4 \quad (\text{S15})$$

9. The free energy is corrected using the Lorentz correction to account for the contributions from the local electric field:

$$\begin{aligned} \alpha &= c_3^2\alpha'P^2 + \frac{c_3c_4}{2\epsilon_0}P^2 \\ \beta &= c_3^3\beta'P^4 \\ A_P(P) &= \alpha P^2 + \beta P^4 \end{aligned} \quad (\text{S16})$$

TABLE S2. Classification of materials based on their transition temperatures

Material	Relation between T_C and T_1	Examples
Ferroelectric	$T_C > T_1/2$	BaTiO_3 , PbTiO_3 , etc.
Quantum paraelectric	$0 < T_C < T_1/2$	SrTiO_3 , KTaO_3 , etc.
Paraelectric	$T_C < 0$	EuTiO_3 , NaMnF_3 , etc.

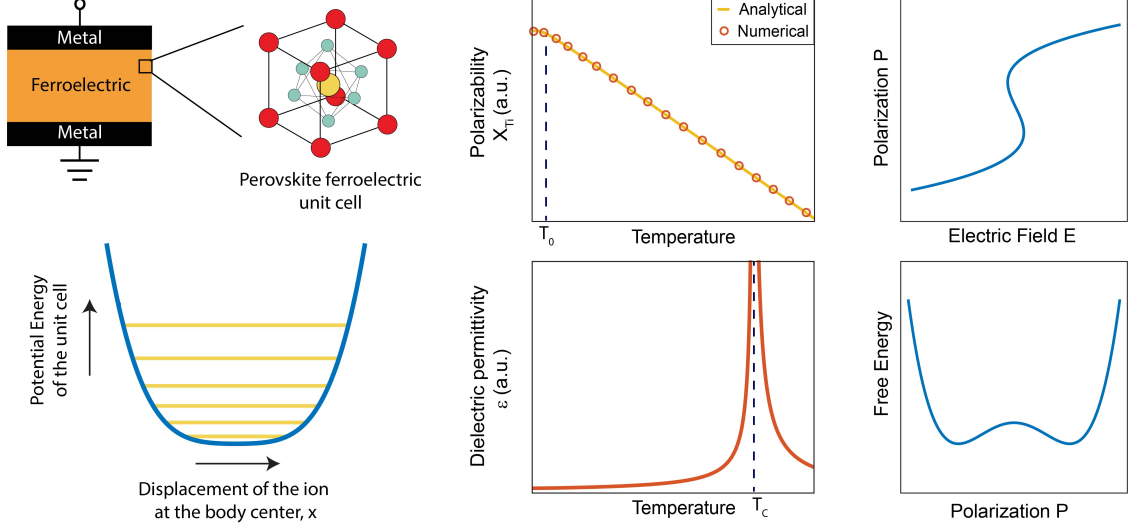


FIG. S2. (a) MFM structure and body-center cubic perovskite unit cell. (b) Anharmonic potential energy of the body-center ion as a function of the displacement x with quantized energy levels.(representative) (c) Ionic polarizability from numerical calculations overlaid on Eq. 2.[2] (d) Temperature-dependence of dielectric permittivity with phase transition at T_C . (e&f) P-E curve and free energy landscape at $T < T_C$

III. FERROELECTRIC-PARAELECTRIC HETEROSTRUCTURES

Consider a FE-PE heterostructure consisting of the ferroelectric and paraelectric layers described by the parameters $[M_F, T_{1F}$ and $T_{CF}]$ and $[M_P, T_{1P}$ and $T_{CP}]$, respectively.

$$\epsilon_P = \frac{M_P}{\frac{T_{1P}}{2} \coth\left(\frac{T_{1P}}{2T}\right) - T_{CP}} \quad (\text{S17})$$

$$\epsilon_F = \frac{M_F}{\frac{T_{1F}}{2} \coth\left(\frac{T_{1F}}{2T}\right) - T_{CF}} \quad (\text{S18})$$

For a thickness ratio r , the heterostructure has an effective dielectric permittivity ϵ_{FP} which can be expressed in terms of Eq. 2 with effective parameters M_{FP} , T_{1FP} and T_{CFP} as shown below.

$$\frac{1+r}{\epsilon_{FP}} = \frac{1}{\epsilon_F} + \frac{r}{\epsilon_P} \quad (\text{S19})$$

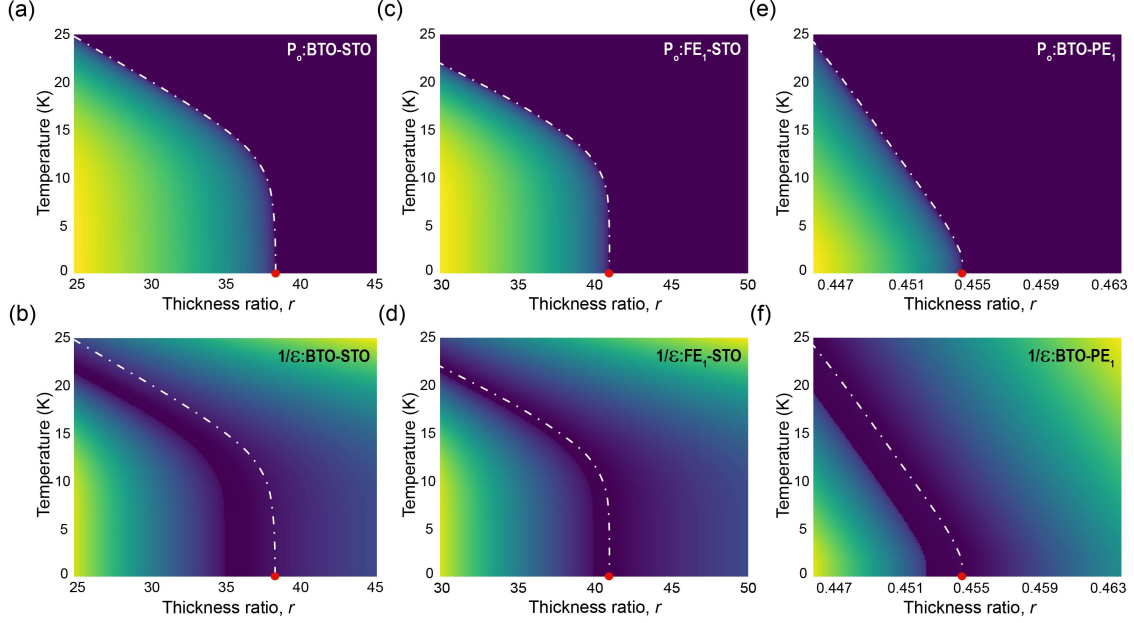


FIG. S3. Remanent polarization P_o and Inverse dielectric polarization $1/\epsilon$ of (a-b) BTO-STO, (c-d) $\text{FE}_1(T_1 = 50 \text{ K}, T_C = 390 \text{ K}, M = 1.5 \times 10^5 \times \epsilon_o \text{ K})$ -STO and (e-f) BTO- $\text{PE}_1(\epsilon_P = 200)$. The red dot indicates the quantum critical point *i.e.* thickness ratio $r = r_C$ at which the FE-PE heterostructure transitions from ferroelectric to paraelectric phase at 0 K

where,

$$\epsilon_{FP} = \frac{M_{FP}}{\frac{T_{1FP}}{2} \coth\left(\frac{T_{1FP}}{2T}\right) - T_{C_{FP}}} \quad (\text{S20})$$

The effective Curie temperature T'_C of this FE-PE heterostructure is:

$$T'_C = \frac{M_P T_{C_F} + r T_{C_P} M_F}{M_P + r M_F} \quad (\text{S21})$$

The critical thickness ratio, r_C , above which the FE-PE heterostructure transitions from being a ferroelectric to a quantum paraelectric at 0 K is found to be,

$$r_C = -\frac{M_P (2T_{C_F} - T_{1_F})}{M_F (2T_{C_P} - T_{1_P})} \quad (\text{S22})$$

Fig. S3 shows the phase diagram and quantum critical points for three different heterostructures including BTO-STO. The microscopic parameters (a, b, c_3, c_4) for BTO are estimated from the first principle *ab initio* calculations of temperature-pressure phase diagrams in Ref. [3], and for STO, these parameters obtained from experiments reported in Ref. [4, 9]. The

parameters are listed in supplementary table S1, and the parameter estimation procedure is described in supplementary section I. It can be seen that the effective quantum temperature of BTO-STO is larger than that of BTO, thereby providing better accessibility to quantum critical region.

- [1] J. Slater, *Physical Review* **78**, 748 (1950).
- [2] J. H. Barrett, *Physical Review* **86**, 118 (1952).
- [3] R. Roussev and A. Millis, *Physical Review B* **67**, 014105 (2003).
- [4] H. Fujishita, S. Kitazawa, M. Saito, R. Ishisaka, H. Okamoto, and T. Yamaguchi, *Journal of the Physical Society of Japan* **85**, 074703 (2016).
- [5] T. Katsufuji and H. Takagi, *Phys. Rev. B* **64**, 054415 (2001).
- [6] R. M. Dubrovin, L. N. Alyabyeva, N. V. Siverin, B. P. Gorshunov, N. N. Novikova, K. N. Boldyrev, and R. V. Pisarev, *Phys. Rev. B* **101**, 180403 (2020).
- [7] S.-P. Shen, J.-C. Wu, J.-D. Song, X.-F. Sun, Y.-F. Yang, Y.-S. Chai, D.-S. Shang, S.-G. Wang, J. F. Scott, and Y. Sun, *Nature communications* **7**, 1 (2016).
- [8] M. J. Haun, E. Furman, S. Jang, H. McKinstry, and L. Cross, *Journal of Applied Physics* **62**, 3331 (1987).
- [9] O. G. Vendik and S. P. Zubko, *Journal of Applied Physics* **82**, 4475 (1997).